Journal of Alloys and Compounds 517 (2012) 1–8

Contents lists available at SciVerse ScienceDirect

Journal of Alloys and Compounds

journal homepage: www.elsevier.com/locate/jallcom

Influence of surfactant CTAB on the electrochemical performance of manganese dioxide used as supercapacitor electrode material

Huaihao Zhang, Yaqiong Wang*, Changwei Liu, Haitao Jiang

College of Chemistry and Chemical Engineering, Yangzhou University, Yangzhou 225002, PR China

ARTICLE INFO

Article history:
Received 8 August 2011
Received in revised form 7 November 2011
Accepted 9 November 2011
Available online 17 November 2011

Keywords:
Surfactant
Manganese Dioxide
Supercapacitor
CTAB

ABSTRACT

MnO_2 nano hollow sphere was prepared by liquid co-precipitation with different concentrations of cationic surfactant CTAB. The morphology and structure of the prepared MnO_2 were investigated by X-ray diffraction (XRD), scanning electron microscopy (SEM), infrared spectroscopy (FT-IR) and low temperature nitrogen adsorption. It was revealed that the obtained manganese dioxide was α-MnO_2 and the particle size of samples was between 100 and 300 nm. As evidenced by the cyclic voltammetry and galvanostatic charge/discharge test, 0.014 mol/L was found to be the optimum impact concentration of CTAB. The MnO_2 synthesized under optimum conditions showed the specific capacitance 178 F/g at the current density of 500 mA/g and its BET area is 229.8 m^2/g, compared to the 126 F/g and 178.4 m^2/g of the MnO_2 synthesized without surfactant.

1. Introduction

Supercapacitor is a new energy storage device with high charging and discharging efficiency, long cycle life, predictable and easily monitored electrical behavior, low sensitivity to temperature and high power density [1]. Therefore, supercapacitor has been applied and shows potential application in communications, transportation, consumer electronics, aviation and so on. Depending on the charge storage mechanism, the supercapacitors can be classified into two categories: electrochemical double layer capacitor (EDLC) and pseudocapacitors. The EDLC has a lower specific capacitance than an optimal pseudo capacitor, because the redox pseudocapacitance can be generated not only on the electrode surface but also within the electrode. The pseudocapacitance is charged by chemisorptions of working cation of the electrolyte at a reduced complex at the surface of the electrode [2]. In recent years, metal oxides such as RuO_x [3], NiO [4] and CoO [5] and MnO_2 [6] have been investigated intensively for pseudocapacitor. Among these metal oxides, manganese oxide is the most promising candidate for supercapacitor electrode because of its low cost, favorable pseudocapacitive characteristics and environmentally benign nature [7]. There are a lot of reports about the manganese oxide used as the electrode material of supercapacitor. Staiti and Lufrano [8] developed and electrochemically investigated a hybrid supercapacitor based on manganese oxide, activated carbon and polymer electrolyte. The specific capacitance of hybrid supercapacitor was 48 F/g (192 F/g as a mean one electrode capacitance), in which that of the positive electrode was 384 F/g of MnO_2 and that of negative electrode 117 F/g of carbon. Vargas et al. [9] prepared briniest-type MnO_2 nanowires by direct reaction of $NaMnO_4$ with ethanol under hydrothermal conditions, specific capacitance of the nanowires is 191 F/g. Dubal et al. [10] used a facile chemical bath deposition (CBD) technique for the preparation of Mn_3O_4 thin films at room temperature, the Mn_3O_4 films when used in supercapacitor exhibited specific capacitance of 284 F/g in 1 M Na_2SO_4 electrolyte.

It is well-known that manganese dioxide can exist in different structural formations, such as α-, β-, γ- and δ-types [11]. For the α-MnO_2, the octahedron MnO_6 into a close-packed hexagonal, it is generally believed that there are some large ions, such as K^+, Ba^{2+}, in the (2 × 2) tunnel, which play a role in stabilizing the tunnel structure. In β-MnO_2, the basic structural unit octahedral MnO_6 form the (1 × 1) tunnel, the gap area of (1 × 1) tunnel is small, it is not conducive to diffusion of ion. δ-MnO_2 is a kind of crystalline compounds with layered structure. In γ-MnO_2, the crisscross growth of (1 × 1) tunnel and (2 × 2) tunnel form a close-packed hexagonal structure [12]. The electrochemical performance of MnO_2 strongly depends on its particle size, morphology, crystalline structure and bulk density. Thus, the study of manganese oxide electrode materials focus on how to change its morphology to improve its electrochemical performance. Surfactant was widely used for preparation of various electrode materials due to its special properties. Li et al. [13] prepared α-MnO_2 nanorods by chemical precipitation in the presence of surfactant. The specific capacitance of the α-MnO_2 electrode has reached to 166.2 F/g at a current density of 200 mA/g in a solution of 1 M Na_2SO_4, however, the concentration of CTAB not been studied in this paper.

* Corresponding author. Tel.: +86 13801452061; fax: +86 051487975244.
E-mail address: qiongyd@126.com (Y. Wang).

0925-8388/$ – see front matter © 2011 Elsevier B.V. All rights reserved.
doi:10.1016/j.jallcom.2011.11.042

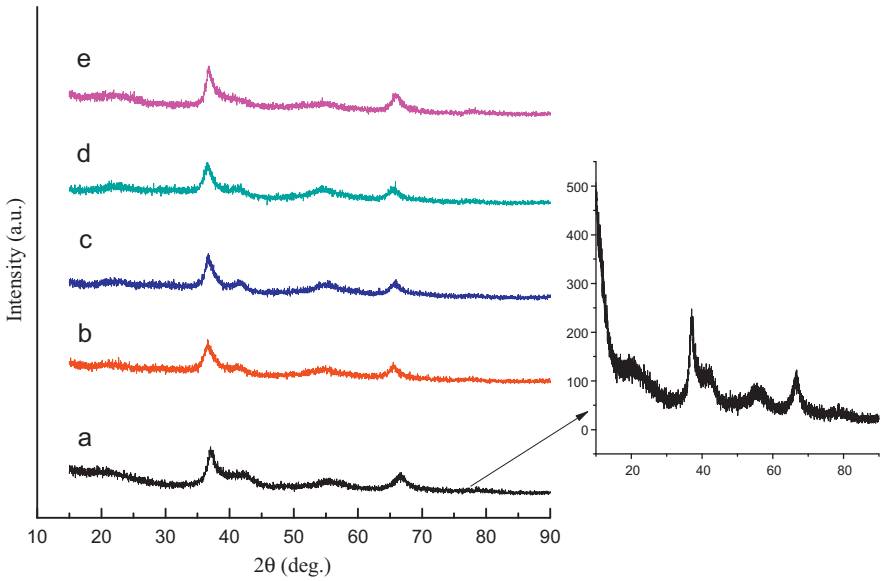

Fig. 1. XRD patterns of MnO_2 prepared at different concentrations of CTAB (Page 5).

Zhou et al. [14] employed non-ionic surfactant F127 to enhance the mesoporosity of carbon aerogel (CA) for electric double layer capacitor application. Jiang et al. [15] synthesized nanostructured MnO_2 by co-precipitation in the presence of Pluronic P123 surfactant. The nanostructured MnO_2 with optimized synthetic conditions gave a large pseudocapacitance of 176 F/g. Zhao et al. [16] used surfactant N-methylpyrrolidone (NMP) assisted electrochemical deposition of α-cobalt hydroxide for supercapacitors, the as-prepared α-$Co(OH)_2$ shows better electrochemical performance with specific capacitance of 651 F/g in a potential range of −0.1 to 0.45 V. Wu and Wang [17] prepared nickel oxide film with open macropores by anodic deposition in the presence of surfactant CTAB, it shows a very high capacitance of 1110 F/g at a scan rate of 10 mV/s. B. Senthilkumar et al. [18] prepared polythiophenes (PTs) by chemical oxidative polymerization method in presence and absence of three different (cationic–CTAB, anionic–SDS and non-ionic–Triton X-100) surfactants using $FeCl_3$ as oxidant. The PT prepared with TRITRON X-100 exhibited higher specific capacitance of 117 F/g compared to 78 F/g of surfactant free PT by the cyclic voltammetry test. From these reports we can see that there have been many reports about surfactant used in preparing supercapacitor electrode materials. However, the influencing mechanism of the surfactant concentrations has not been full understood. In this study, we prepared manganese dioxide by the liquid co-precipitation method. This is the first report on using different concentrations of cationic surfactant CTAB to control the structure of manganese dioxide and the influence of residual surfactants on the electrochemical properties of materials.

2. Experimental

2.1. Synthesis of manganese dioxide and preparation of electrode

The starting materials for MnO_2 preparation included analytical-grade potassium permanganate ($KMnO_4$), manganese sulfate ($MnSO_4{\cdot}H_2O$) and de-ionized water (DW). First, a specific amount of hexadecyl trimethyl ammonium bromide (CTAB) was solved in DW under continuous stirring. Then 20 ml 0.4 M manganese sulfate solution was added to the CTAB solution. After complete mixing, 30 ml 0.18 M potassium permanganate solution was added drop by drop under stirring. After continuous magnetic stirring for 12 h, as-prepared MnO_2 was collected by centrifugation and vacuum filtration, washed with de-ionized water and ethanol, dried at 80 °C for 12 h, subsequently resulting in black powder. The products prepared using

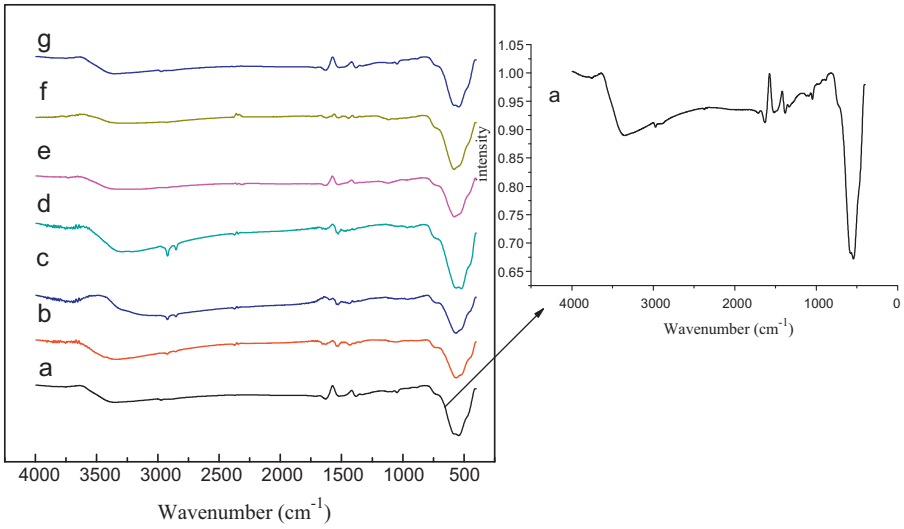

Fig. 2. FT-IR spectra of MnO_2 synthesized with different weights of CTAB (Page 6).

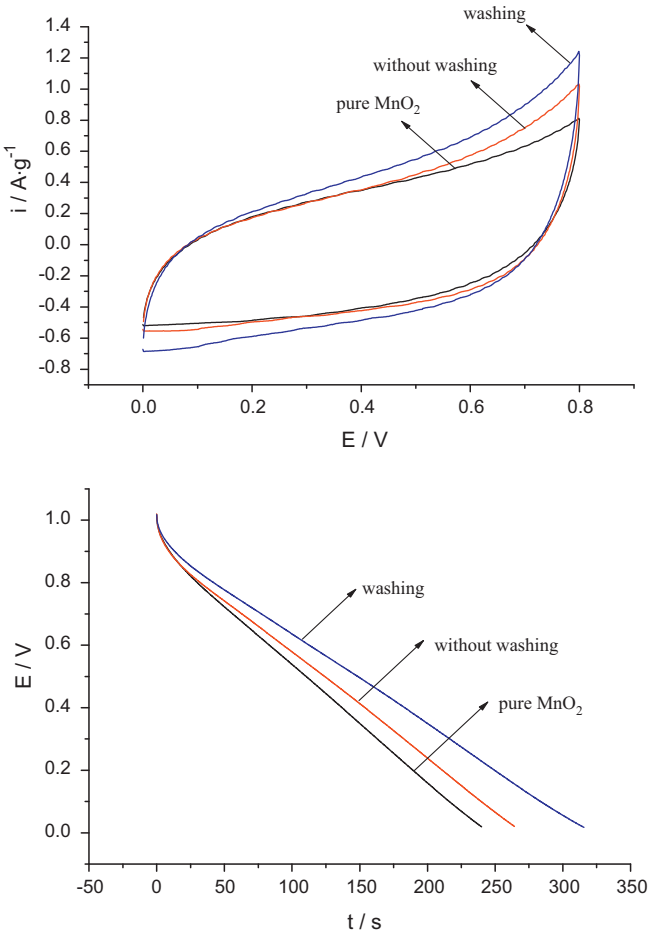

Fig. 3. Galvanostatic charge/discharge profiles of MnO_2 prepared at different weights of CTAB at the current density of 500 mA/g (Page 6).

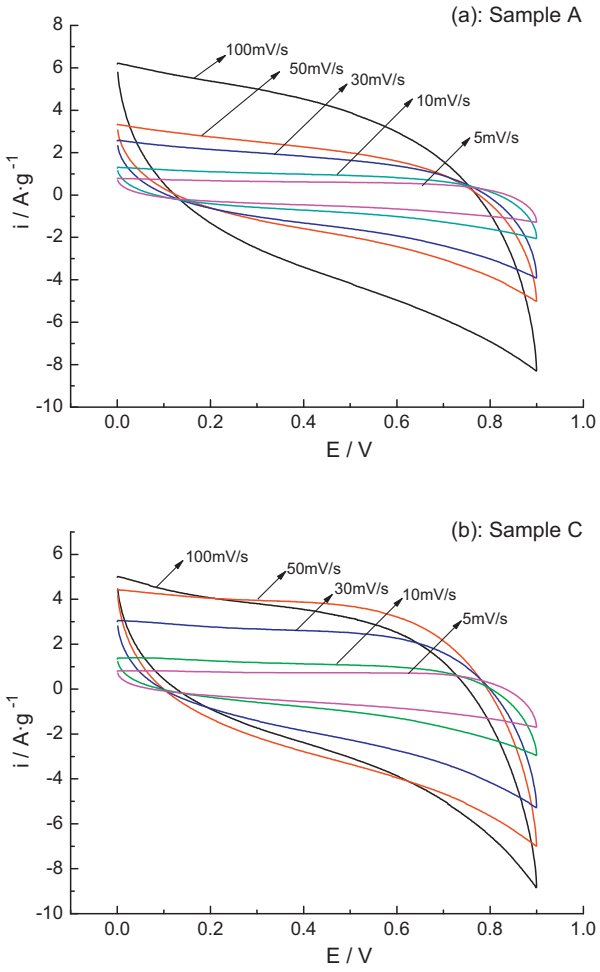

Fig. 4. Cyclic voltammograms of MnO_2 at different scan rates: (a) sample A and (b) sample C (Page 7).

different CTAB dosages are denoted as sample A (0 g), B (0.05 g), C (0.1 g), D (0.2 g), E (0.3 g), F (0.4 g) and G (0.8 g). As for electrode fabrication, the as-prepared MnO_2, conducting agent graphite and binder (60 wt% PTFE) were mixed by weight ratio of 85:10:5. Then, an appropriate amount of ethanol was added into the mixture and stirred into a paste. The paste was smeared into a 1 cm^2 area foam nickel mesh. Subsequently, the mesh was dried in air at 90 °C for 4 h to remove the solvent and finally was pressed under the pressure of 10 MPa to keep good adherence between the electrode material and the nickel mesh current collector. The fabrication process for carbon electrode is the same to MnO_2 electrode.

2.2. Structural characterization

The crystalline phase of sample was tested by Bruker AXS D8 ADVANCE X-ray diffractometer with Cu K_α radiation (λ = 1.5406 Å). Diffraction data were collected in the 2θ range from 10° to 90°, the generator current was 200 mA and the generator voltage was 40 kV. Fourier transform infrared (FT-IR) spectra of the samples were recorded on a Bruker Tensor 27 spectrometer using KBr as dispersing medium. The morphology of the obtained manganese oxide powder was observed using a Philips XL-30 field emission scanning electron microscope (FESEM). The BET surface area of sample was measured by low temperature nitrogen adsorption apparatus (sorptomatic 1990, American Thermal Power Corporation).

2.3. Electrochemical characterization

All the electrochemical measurements concerned were carried out in 0.5 M K_2SO_4 aqueous electrolyte using a three-electrode system. Carbon and saturated calomel electrode (SCE) were used as counter electrode and reference electrode, respectively. Cyclic voltammetry (CV) were performed within a potential range of 0–0.9 V versus SCE at a scan rate from 5 mV/s to 100 mV/s on the CHI 660B electrochemical workstation (Chenghua, Shanghai China). Constant current charge and discharge tests were also conducted at current densities from 300 mA/g to 5000 mA/g between 0 V and 1.0 V versus SCE. Electrochemical impedance spectroscopy (EIS) analyses of the MnO_2 electrode were determined with the AutoLab-PGSTAT30 electrochemical workstation, AC amplitude of 5 mV being applied in a frequency range of 0.01–10^5 Hz.

3. Results and discussion

3.1. X-ray diffraction patterns and FT-IR spectra of samples

Fig. 1 shows the XRD patterns of MnO_2 prepared at different concentrations of CTAB. The figure shows the addition of surfactant CTAB in the preparation process has no effect on the crystalline phase of MnO_2, the intensity of all samples XRD peaks are weak and severely broaden, which indicate a small degree crystallization of samples and a typical amorphous structure [19]. MnO_2 material with this structure is more suitable for the supercapacitor electrode material [20]. The amorphous structure is conducive to proton de-embedded and embedded rapidly, result in a rapid, reversible chemical absorption/desorption or oxidation–reduction reaction in the electrode surface or within the bulk phase, and then generate pseudocapacitance. This will not cause serious deformation of the structure of the electrode material and does not affect on the performance of electrode [21]. Comparison of the diffraction peak at 2θ = 37.2° matches α-MnO_2 according to a standard JCPDS card (44-0141). It confirms that the obtained manganese oxide is main microcrystalline α-MnO_2. The tunnel of α-MnO_2 can accept cations with radius up to 0.15 nm, such as K^+, NH_4^+, etc. these cations play a role in stabilizing the structure. The γ-MnO_2 and β-MnO_2 with smaller tunnel can only accept a small radius particle

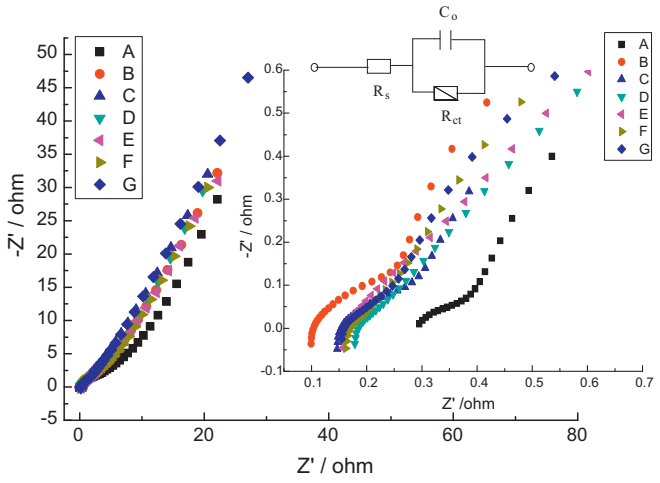

Fig. 5. The AC impedance curves of MnO_2 prepared at different weights of CTAB and the equivalent circuit diagram of electrode: C_0, equivalent ideal capacitors; R_S, equivalent series resistance; R_{ct}, faraday resistance of electrode (Page 7).

such as H^+ ions. When a solution exists K^+, NH_4^+, etc., it can induce the formation of α-MnO_2 [22].

Fig. 2 gives the FT-IR spectra of the obtained MnO_2. At the wave number of 3400 cm^{-1}, there are the H–O–H stretching vibration and bending vibration absorption peak. The absorption bands observed at 1425 cm^{-1} and 1630 cm^{-1} are usually ascribed to the hydroxyl of physically adsorbed water or crystal water in the samples. The broad absorption bands at 400–800 cm^{-1} are attributed to the characteristic peak of MnO_6 octahedron of α-MnO_2 [23–25]. The FT-IR spectra of MnO_2 prepared at different concentrations of CTAB have no significant difference. There is no absorption peak of other organic functional groups found in the FT-IR spectra.

3.2. Electrochemical properties of the MnO_2 electrode

The galvanostatic charge/discharge profiles of MnO_2 prepared at different adding amount of CTAB at the current density of 500 mA/g were determined in an electrochemical window of 1.0 V, as shown in Fig. 3. It can be observed the charge/discharge profiles of the sample shows an isosceles triangle shape and the potential–time relationships are all approximately linear, which indicates that the MnO_2 electrodes have regular capacitive behaviors and good cycling stabilities. There is a significant voltage drop at the very beginning of discharge process due to the system resistance.

According to the formula of specific capacitance:

$$C = \frac{I\Delta t}{m\Delta V}$$

where I is the current of charge/discharge, t is the time of discharge, ΔV is 1.0 V, and m is the mass of active materials in the working electrode [26–28]. Table 1 shows the specific capacitance of the seven samples at the current density of 500 mA/g.

Generally speaking, the specific capacitance decreases with the increase of current density for all seven samples, while the decrease tendency varies from different samples. Sample C with 178 F/g at the current density 500 mA/g shows the highest capacitance among all seven samples, which is larger than sample A by 41.3%. When the current density increases from 300 mA/g to 5000 mA/g, the capacitance of sample C decreases from 197 F/g to 80 F/g, dropping by 59.4%. By contrast, the other samples dropped by 77.8% (A), 67.9% (B), 72.5% (D), 76.8% (E), 77.1% (F), 69.0% (G) respectively. These results indicate the optimum concentration of CTAB is 0.014 mol/L.

Fig. 4 shows the CV curves of samples at different scan rates from 5 mV/s to 100 mV/s over the voltage range of 0.0–0.9 V versus

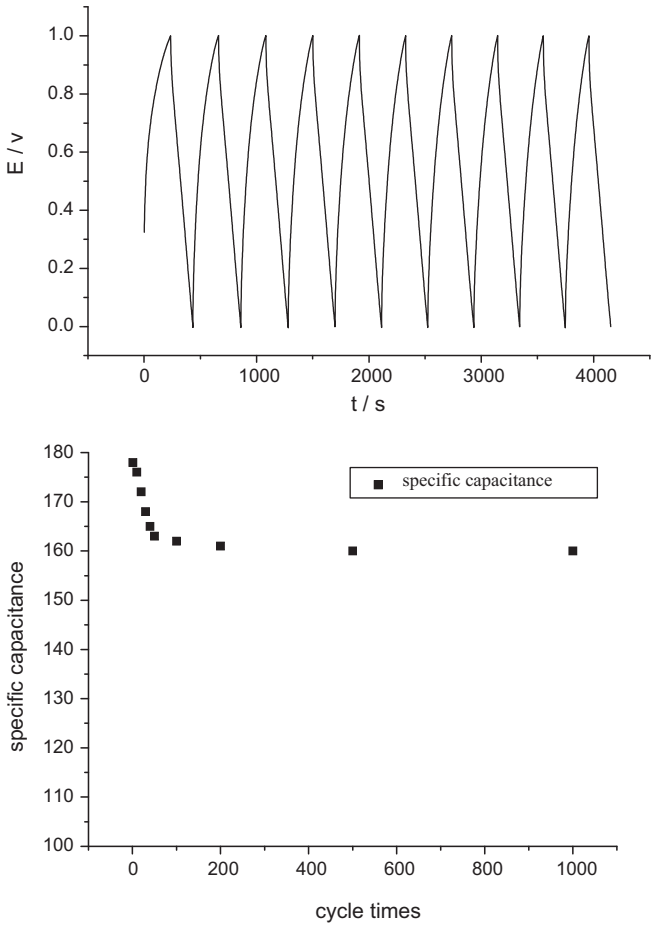

Fig. 6. Cyclic performance of the MnO_2 electrode (Page 8).

SCE in 0.5 M K_2SO_4 solution. As shown in Fig. 4(a), with the increase of the scan rates, the CV curve of the sample A quickly becomes a deformed rectangle from the beginning relatively regular rectangle, and finally into the oval. This coincided with the fact that the specific capacitance of the sample decreases as the scanning speed increases, the material presents a poor rate capability. However the response current of the sample C increases correspondingly with the scan rate increase, indicating that the sample presents good

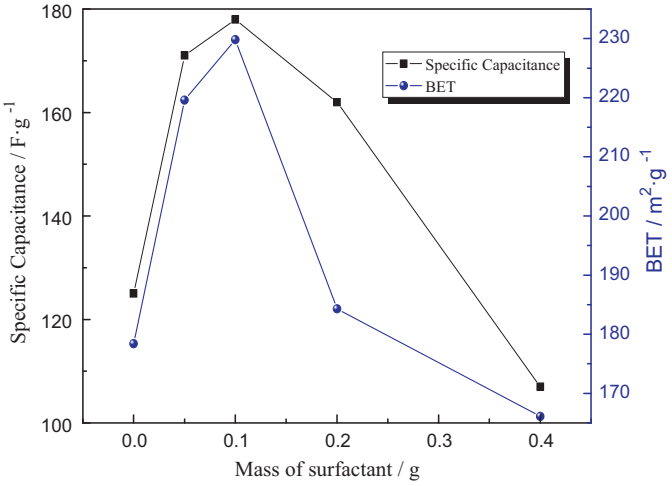

Fig. 7. Influence of surfactant mass on the BET area and discharge capacitance (Page 8).

Table 1
Specific capacitance of MnO_2 prepared at different concentrations of CTAB at different current densities (Page 7).

Current density (mA/g)	Specific capacitance (F/g)						
	A	B	C	D	E	F	G
300	185	196	197	182	155	131	116
500	126	177	178	162	120	107	104
1000	88	134	146	120	90	80	81
2000	59	101	117	87	67	56	61
5000	41	63	80	50	36	30	36

capacitance performance and rate capability, and the electrode has good dynamics [29].

Equivalent series resistance (ESR) is one of the important evaluating indicators of supercapacitor [30]. The equivalent circuit diagram of electrode is shown in Fig. 5. The AC impedance curve at high frequency was an irregular semicircle, and this shows the electrode process at high frequencies is under electrochemical polarization control. The size of the semicircle diameter indicates the size of electrode reaction resistance. Intercept of the curve in the *X*-axis represents the equivalent series resistance of electrode. The

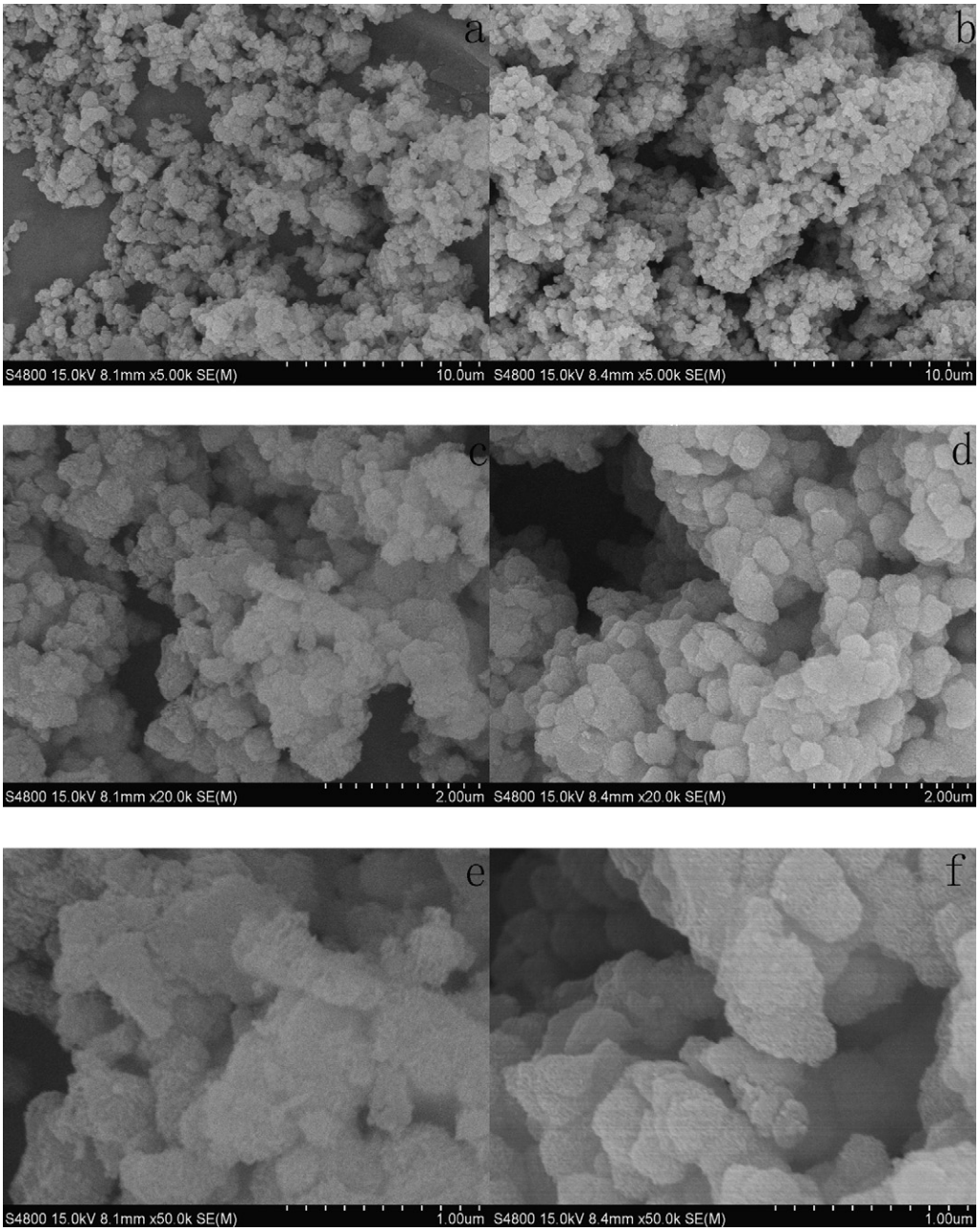

Fig. 8. SEM images of the obtained MnO_2 powder under different magnification (a and b) 5000×; (c and d) 20,000×; (e and f) 50,000×; (a, c and e) sample A; and (b, d and f) sample C (Page 9).

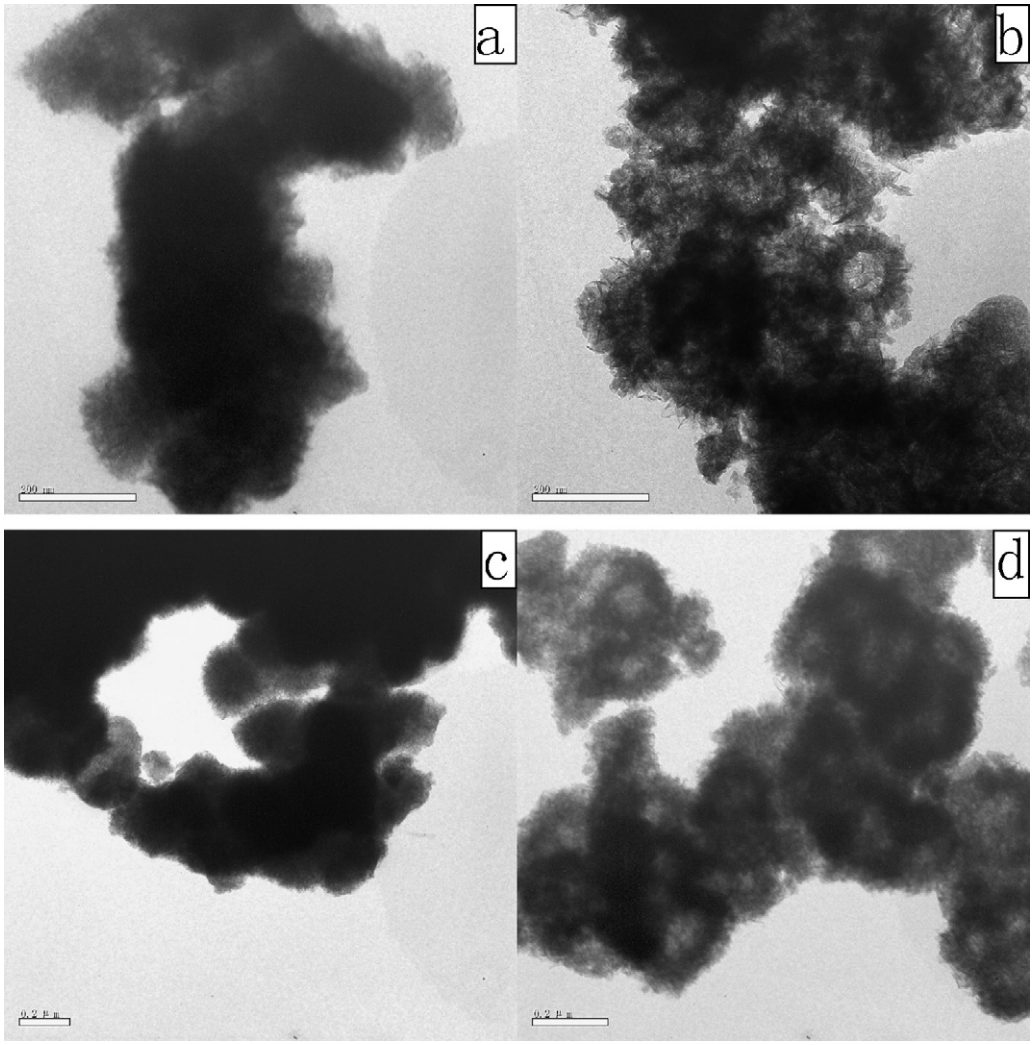

Fig. 9. TEM images of the obtained MnO_2 powder under different magnifications (a and b) 97,000×; (c and d) 59,000 (a and c) sample A; and (b and d) sample C (Page 9).

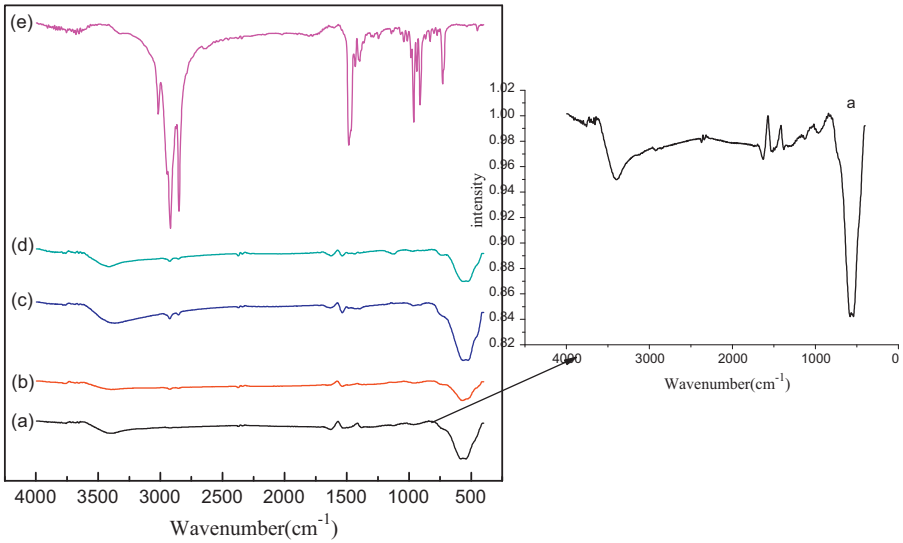

Fig. 10. FT-IR spectra of samples with different degrees of washing (a), pure MnO_2; (b), sample washed by deionized water and ethanol; (c), sample washed by deionized water; (d), unwashed sample; and (e), pure CTAB (Page 10).

line in the low-frequency part indicated that the electrode process is under diffusion control. The speed of double layer formation on the surface of the electrode materials can be characterized by the slope of the line. The larger the linear slope is, the faster the electric double layer formed [31,32]. It can be seen from the Fig. 5 that the ESR of electrode decreases because of the surfactant CTAB added generally, which is probably due to that the surfactant reduced agglomeration of manganese dioxide particles and increased the specific surface area of material.

The cyclic performance of electrode was investigated by the charge–discharge test. 10 cycles of charge–discharge of the MnO_2 electrode at the current density 500 mA/g are shown in Fig. 6. It can be seen that the charge–discharge curve can maintain a good symmetry, the potential–t relationships on charge–discharge profiles are all approximately linear. It have been calculated, after 10 and 500 cycles of charge–discharge, the specific capacitance decreased by 1.3% and 10.1% respectively, compared to the initial capacitance. After 500 cycles, the specific capacitance of electrode tends to stabilization. This indicates that the electrode has regular capacitive behavior and good cycling stability.

3.3. The relationship between the physical characteristics and electrochemical properties of materials

The main charge storage mechanism of manganese dioxide in neutral electrolyte is the embedding and desorption behavior of electrolyte cation in the surface layer and bulk of manganese dioxide and related to the role of amount of hydrates on the electrolyte cations diffusion [33]. So the specific surface area and pore structure of sample are important physical characteristics affecting its electrochemical properties.

Fig. 7 shows the influence of surfactant dosage on the BET surface area and discharge capacitance. With the increase of surfactant dosage from 0.0 to 0.4 g, the BET area of samples increased from 178.4 m^2/g to 229.8 m^2/g, and then decreased to 166.1 m^2/g. The varying tendency of specific capacitance is same to that of BET surface area. The results obtained above indicated that samples with larger specific area have higher specific capacitance, which may be attributed to that the redox reaction of electrode mainly occurs on the surface of material [34]. This also explained the addition of CTAB increased the specific surface area of sample, which in turn increased surface redox reactions and the specific capacitance. The MnO_2 synthesized under optimum conditions possesses the BET surface area of 229.8 m^2/g and also exhibits a high specific capacitance of 178 F/g at the current density of 500 mA/g.

Fig. 8 gives the SEM images of the obtained powder under different magnifications. Fig. 8a, c and e presents the sample C, Fig. 8d–f presents the sample A. It can be seen from Fig. 8 that the synthesized samples are irregular particles. Samples were also examined by transmission electron microscopy. As can be seen from the TEM images with magnification 59,000× and 97,000× shown in Fig. 9. Sample A shows a solid spherical particle with very short burrs in the surface compared to a hollow sphere with long burrs of sample C. The particle size of samples ranges from 100 nm to 300 nm. The burrs of sample C are longer and denser and the particles distribute more evenly than sample A under the same magnification. The hollow structure of sample C may be the reason of its high specific capacitance. The addition of surfactant CTAB can reduce agglomeration of manganese dioxide particles and make it distribute more evenly. This is mainly related to the formation process of manganese dioxide crystal nucleus. In the absence of surfactant, the reaction between potassium permanganate and manganese sulfate generates crystal nuclei first, manganese dioxide nuclei grow as the reaction continues, and ultimately irregular particles with coarse surface forms. In the presence of surfactant CTAB, divalent manganese ions and CTAB forms complex by the interactions between

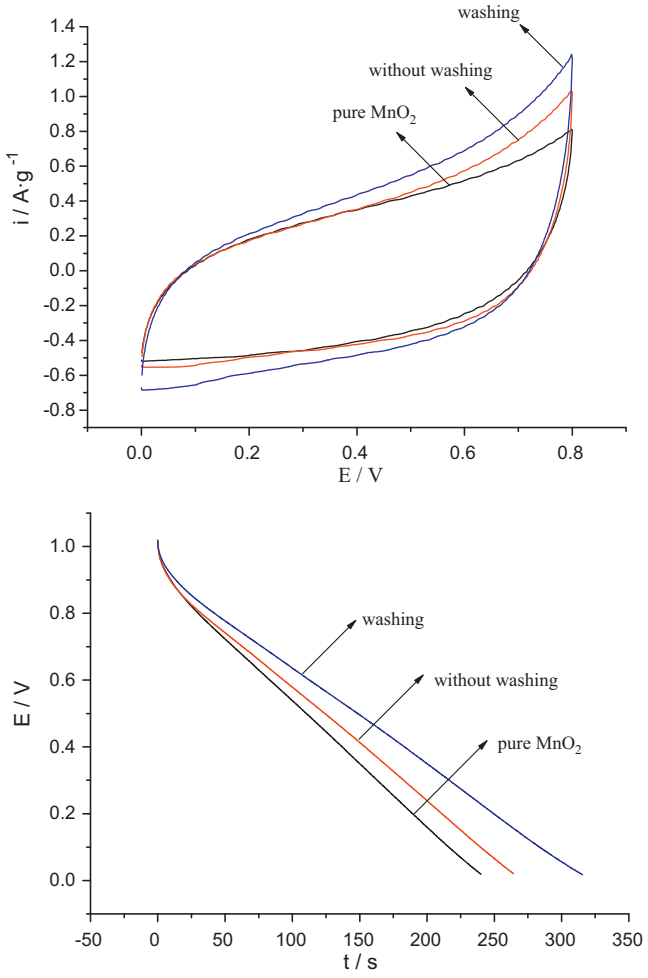

Fig. 11. CV curves and constant current discharge curves of samples with different degrees of washing (Page10).

ions at the beginning, afterward manganese dioxide grows along a specific direction, which is controlled by the surfactant [35,36].

3.4. The influence of CTAB residue

If the surfactant is not removed in the process of washing and separation, what impact will be engendered on the performance of material? We investigated the influence of residual surfactants on the electrochemical properties of materials. The samples with different washing degrees were tested by FT-IR, cyclic voltammetry and galvanostatic charge–discharge. The results are shown in Figs. 10 and 11. At the wave number from 2850 cm^{-1} to 2960 cm^{-1} of the FT-IR spectra b–e, there are the stretching vibration peaks of saturated hydrocarbons of $-CH_3$ and $-CH_2$ attributed to the long hydrocarbon chain of CTAB. It can be seen that the surfactant CTAB cannot be completely removed in the washing process, this is not consistent with the conclusions in the literature [15]. It can be seen the CTAB residue makes the specific capacitance of material decrease slightly from 168 F/g to 147 F/g in Fig. 11. Thus, from the perspective of industrial applications, the prepared manganese dioxide may not necessary need to be washed.

4. Conclusions

It is demonstrated in this paper that the surfactant CTAB has certain impacts on the electrochemical properties of MnO_2. The obtained manganese dioxide is mainly composed of α-MnO_2, the

particle size of samples ranged from 100 nm to 300 nm. The MnO_2 synthesized under optimum conditions (sample C) shows a specific capacitance 178 F/g at the current density of 500 mA/g, which is higher than the MnO_2 synthesized without surfactant (sample A) by 41.3%. The BET surface area of the optimized sample is 229.8 m^2/g, which is larger than sample A by 28.8%. The MnO_2 synthesized under optimum conditions also has a good rate capability. The BET surface area and SEM images of material indicate that the surfactant introduced in the preparation process of MnO_2 can reduce the agglomeration of manganese dioxide particles, make it distributed more evenly and increase the BET surface area of sample. These results indicate that surfactant CTAB can improve the electrochemical performance of MnO_2 electrode, and an optimum concentration for CTAB does exist. The CTAB residue makes the specific capacitance of material decrease slightly, and may not necessary need to be washed.

References

[1] M. Conte, Fuel 10 (2010) 806.
[2] H.Y. Lee, J.B. Goodenough, J. Solid State Chem. 144 (1999) 220.
[3] J.J. Jow, H.J. Lee, H.R. Chen, M.S. Wu, T.Y. Wei, Electrochim. Acta 52 (2007) 2625.
[4] K.W. Nam, E.S. Lee, J.H. Kim, J. Electrochem. Soc. 152 (2005) A2123.
[5] C. Lin, J.A. Ritter, B.N. Popov, J. Electrochem. Soc. 145 (1998) 4097.
[6] M.S. Wu, P.C. Julia, Electrochem. Solid-State Lett. 7 (2004) A123.
[7] C.J. Xu, F.Y. Kang, B.H. Li, H.D. Du, J. Mater. Res. 25 (2010) 1421.
[8] P. Staiti, F. Lufrano, Electrochim. Acta 55 (2010) 7436.
[9] O.A. Vargas, A. Caballero, L. Hernán, J. Morales, J. Power Sources 196 (2011) 3350.
[10] D.P. Dubal, D.S. Dhawale, R.R. Salunkhe, V.J. Fulari, C.D. Lokhande, J. Alloys Compd. 497 (2010) 166.
[11] Y.C. Chen, Z.Y. Duan, Y.L. Min, M.W. Shao, Y.G. Zhao, J. Mater. Sci. Mater. Electron. 22 (2011) 1162.
[12] S.R. Segal, S.L. Suib, L. Foland, Chem. Mater. 9 (1997) 2526.
[13] Y. Li, H.Q. Xie, J.F. Wang, L.F. Chen, Mater. Lett. C5 (2011) 403.
[14] J.H. Zhou, Y.J. Ji, J.P. He, C.X. Zhang, G.W. Zhao, Microporous Mesoporous Mater. 114 (2008) 424.
[15] R.R. Jiang, T. Huang, J.L. Liu, J.H. Zhuang, A.S. Yu, Electrochim. Acta 54 (2009) 3047.
[16] T. Zhao, H. Jiang, J. Ma, J. Power Sources 196 (2011) 860.
[17] M.S. Wu, M.J. Wang, Chem. Commun. 46 (2010) 6968.
[18] B. Senthilkumar, P. Thenamirtham, R. Kalai Selvan, Appl. Surf. Sci. 257 (2011) 9063.
[19] Z.A. Zhang, B.C. Yang, J. Funct. Mater. Devices 11 (2005) 58 (in Chinese).
[20] J.P. Zheng, P.J. Cygan, T.R. Jow, J. Electrochem. Soc. 142 (1995) 2699.
[21] B.C. Yang, Z.A. Zhang, Electron. Compon. Mater. 24 (2005) 33 (in Chinese).
[22] L.S. Suib, Acc. Chem. Res. 41 (2008) 479.
[23] D.L. Fang, B.C. Wu, A.Q. Mao, Y. Yan, C.H. Zheng, J. Alloys Compd. 507 (2010) 526.
[24] Z.H. Ai, L.Z. Zhang, F.H. Kong, H. Liu, W.T. Xing, J.R. Qiu, Mater. Chem. Phys. 118 (2008) 162.
[25] M.V. Ananth, S. Pethkar, K. Dakshinamurthi, J. Power Sources 75 (1998) 278.
[26] Y. Zhang, H. Feng, X.B. Wu, L.Z. Wang, A.Q. Zhang, T.C. Xia, Int. J. Hydrogen Energy 34 (2009) 4889.
[27] P. Sharma, T.S. Bhatti, Energy Convers. Manage 51 (2010) 2901.
[28] C.Y. Chen, S.C. Wang, C.Y. Lin, F.S. Chen, C.K. Lin, Ceram. Int. 35 (2009) 3469.
[29] Q.T. Qu, P. Zhang, B. Wang, Y.H. Chen, S. Tian, Y.P. Wu, R. Holze, J. Phys. Chem. C 113 (2009) 14020.
[30] G. Zhu, H.J. Li, L.J. Deng, Z.H. Liu, Mater. Lett. 64 (2010) 1763.
[31] Q.X. Zha, An Introduction to Dynamics in Electrode Process, First ed., Science Press, Beijing, 2005, pp. 32–33, (in Chinese).
[32] C.N. Cao, J.Q. Zhang, An Introduction to Electrochemical Impedance Spectroscopy, First ed., Science Press, Beijing, 2002, pp. 68–92, (in Chinese).
[33] M. Ghaemi, F. Ataherian, A. Zolfaghari, S.M. Jafari, Electrochim. Acta 53 (2008) 4607.
[34] S.F. Chin, S.C. Pang, M.A. Anderson, Mater. Lett. 64 (2010) 2670.
[35] L.L. Dai, R. Sharma, C.Y. Wu, Langmuir 21 (2005) 2641.
[36] J.K. Sakata, A.D. Dwoskin, J.L. Vigorita, E.M. Spain, J. Phys. Chem. B 109 (2005) 138.